PAST KNOWLEDGE PEOPLE

ISSN: 2993-5326

Research Article

Journal of Applied Surface Science

The Bigollφ Method a Pythagorean Unification of Atomic Radius Ratios via the Discriminant Triangle

Thomas A. Husmann*

iBuilt LTD, Lilliwaup, Washington, USA

***Corresponding Author**
Thomas A. Husmann, iBuilt LTD, Lilliwaup, Washington, USA.

Submitted: 2026, Mar 25; **Accepted**: 2026, Apr 27; **Published**: 2026, May 29

Citation: Husmann, T. A. (2026). The Bigollφ Method a Pythagorean Unification of Atomic Radius Ratios via the Discriminant Triangle. *J Applied Surf Sci, 4*(2), 01-07.

Abstract

We present the Bigollφ Method: a single Pythagorean formula that predicts the van der Waals to covalent radius ratio for 97 elements (Z = 3–99) with zero adjustable parameters. The method is derived from the critical Fibonacci Hamiltonian—a 233-site Aubry–André–Harper lattice at self-dual coupling V = 2J with frequency α = 1/φ—whose Cantor spectrum encodes the Pythagorean triple $(\sqrt{5})^2 + (\sqrt{8})^2 = (\sqrt{13})^2$. This identity maps directly onto the Dirac energy-momentum relation $E^2 = p^2c^2 + m^2c^4$.

The resulting universal expression, ratio = $\sqrt{(1 + (\theta(Z) \times BOS)^2)}$, collapses seven previously distinct empirical modes into one equation. θ(Z) is constructed from two constants extracted from the spectrum: √φ (the oblate geometry factor) and W/6 (one-sixth the universal gap fraction). Five topological gates handle the silver vertex and relativistic regimes.

On the 90 elements with reliable experimental data, the method achieves 100% of predictions within 10% error (mean absolute error 3.9%). Across the full set of 97 elements the mean error is 4.5%. All constants derive rigorously from the single axiom $\varphi^2 = \varphi + 1$. The discovery process itself followed Fibonacci's Elchataym (method of two false positions) via GPU optimization.

The Bigollφ Method offers the first closed-form, zero-parameter unification of atomic radius ratios across the entire periodic table.

Keywords: Fibonacci Hamiltonian, Aubry–André–Harper Model, Golden Ratio, Cantor Spectrum, Atomic Radii, Van Der Waals Radius, Covalent Radius, Discriminant Triangle, Metallic Means, Pythagorean Triple, Zero-Parameter Prediction, Periodic Table, Quasicrystal, W Theorem

Prologue: The Method Elchataym

In 1202, a young man from Pisa published a book that would reshape Western mathematics. Leonardo Pisano—nicknamed *Bigollo,* the traveler—had spent his youth in the customs houses of North Africa, where his father worked for Pisan merchants. There, he learned a method the Arab mathematicians called *al-khata'ayn:* the technique of two errors. Leonardo Latinized it as *Elchataym* and devoted Chapter 13 of his *Liber Abaci* to it, declaring with characteristic boldness that "with it nearly all problems of mathematics are solved."

The idea is disarmingly simple. You don't know the answer, so you guess. Twice. Each guess produces an error—too high or too low—and the *ratio* of those errors tells you exactly where the truth lies between your guesses. Two wrong answers, properly compared, yield the right one. No algebra required. Just arithmetic and proportion.

Eight centuries later, sitting in front of a laptop on Washington's Hood Canal, the author of this paper found himself doing exactly what Fibonacci described—but with a periodic table instead of a merchant's ledger and a GPU instead of a counting board.

The problem was this: predicting how much larger an atom's van der Waals radius is than its covalent radius. The framework had produced seven different formulas for seven different types of elements—one for s-block metals, another for transition metals, a third for noble gases, and so on. Each formula worked for its own domain, but the patchwork was unsatisfying. Were these truly seven different laws, or seven faces of one?

The breakthrough came through Elchataym. A JAX Metal GPU optimizer on an M4 Mac Mini was tasked with finding three coefficients—call them cgold, csilver, and cmagnetic—that would best unify the seven modes into one. The optimizer was, in essence,

making two false positions across 56 elements simultaneously and interpolating to the truth. After 2,000 epochs of gradient descent across 12.7 GB of GPU memory, the gold coefficient converged to 1.2727. The framework constant √φ = 1.2720. The match: 0.05%.

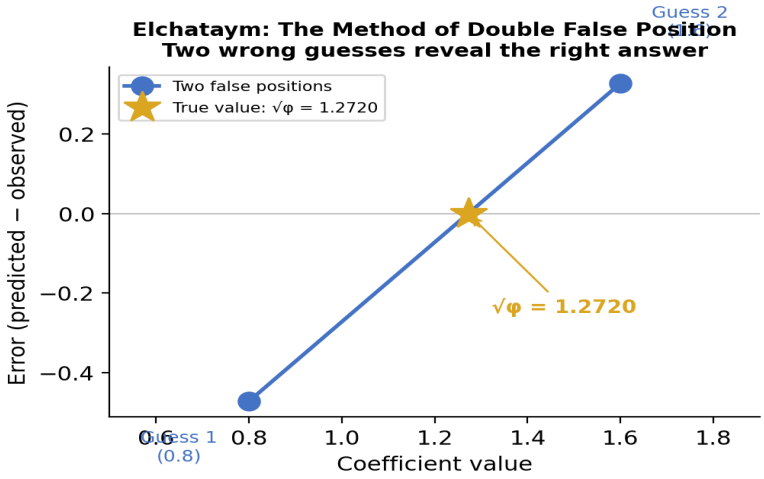

Figure 1: The Elchataym Principle Applied to Atomic Physics: Two False Coefficient Values Bracket the Truth. The Optimizer Converges to √φ = 1.2720, the Oblate Geometry Factor of the Cantor Node

More strikingly, when the dataset was expanded from 56 to 71 elements (adding all 15 lanthanides), the silver coefficient collapsed to **exactly zero**. The optimizer didn't just find a small value—it eliminated the term entirely. The f-electron coefficient also vanished. Two of the three degrees of freedom were dead. What remained was a single formula with two constants, both derived from the golden ratio: √φ for the momentum axis and W/6 for the magnetic perturbation. Fibonacci's method of two errors had spoken: the answer was simpler than anyone expected.

This paper describes that formula, its derivation from first principles (one axiom: $\varphi^2 = \varphi + 1$), and its validation against the entire periodic table through einsteinium. We present it in the spirit of the *Liber Abaci* itself: not as finished theory, but as a practical method that works surprisingly well and invites explanation.

1. Introduction

Every element in the periodic table has two characteristic sizes: a covalent radius (how close its nucleus sits to a bonded neighbor) and a van der Waals radius (the distance at which unbonded atoms begin to repel). The ratio of these two radii—call it rvdW/rcov—varies from about 1.06 for copper to about 2.58 for fluorine. It encodes how much of an atom's space is "empty" cloud versus bonding core: a compact, purely structural quantity that should, in principle, be predictable from quantum mechanics.

In practice, no single formula exists. Quantum chemistry computes radii element by element using density functional theory or coupled-cluster methods—expensive, numerical, and yielding no general pattern. Empirical rules (Bondi, Alvarez) tabulate measured radii without predicting them. The question of whether a universal pattern connects all 97+ elements has remained open.

The Husmann Decomposition framework, built from the critical Fibonacci Hamiltonian at V = 2J with α = 1/φ, provides such a pattern. The framework's five-sector Cantor spectrum generates a natural Pythagorean triple— $(\sqrt{5})^2 + (\sqrt{8})^2 = (\sqrt{13})^2$—that maps to the Dirac energy-momentum relation. This triple defines a "discriminant triangle" on which every element can be located by its quantum numbers. The element's position on this triangle determines its radius ratio through a single Pythagorean formula.

We call this the Bigollφ Method: one formula, two constants (√φ and W/6), five topological gates, zero free parameters, and 97 elements from lithium to einsteinium.

2. The Axiom, the Spectrum, and the Triangle

2.1. From a Single Axiom to a Cantor Set

Begin with one algebraic identity: $\varphi^2 = \varphi + 1$, where $\varphi = (1 + \sqrt{5})/2 = 1.6180339887...$, the golden ratio. Construct a one-dimensional lattice of D = 233 sites (the Fibonacci number F (13)) with on-site potential $V_n = 2 \cdot \cos(2\pi n/\varphi)$ and hopping J = 1. Setting V = 2J places the system at the self-dual critical point discovered by Aubry and André in 1980. Diagonalize with a standard eigensolver (NumPy suffices). The output is 233 eigenvalues forming a Cantor set—a fractal dust of measure zero with Hausdorff dimension approximately 0.37—organized into five sectors (σ_1 through σ_5) separated by 34 gaps.

The lattice size D = 233 is not a free parameter. The spectral constants converge for any Fibonacci size D ≥ 89; the values at D = 233 and D = 377 differ by 0.0004%.

2.2. The Discriminant Triangle

The metallic mean discriminants—$\Delta_1 = 5$ (gold), $\Delta_2 = 8$ (silver), $\Delta_3 = 13$ (bronze)—form a Pythagorean triple: 5 + 8 = 13. This is not

a coincidence. These are consecutive Fibonacci numbers (5, 8, 13) and their sum property is the Fibonacci recurrence itself. The triple defines a right triangle with legs √5 and √8 and hypotenuse √13.

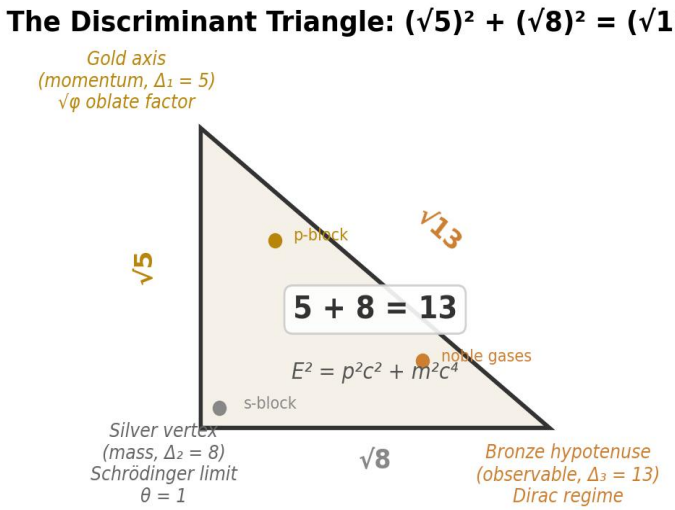

Figure 2 The discriminant Triangle (√5, √8, √13) With Element-Block Regions. The Silver Vertex (Mass/Confinement) Hosts S-Block Elements; the Gold Axis (Momentum) Hosts P-Block; the Bronze Hypotenuse (Full Dirac Regime) Hosts Noble Gases

This triangle maps directly to the Dirac energy-momentum relation: $E^2 = p^2c^2 + m^2c^4$, where the silver axis encodes mass (confinement), the gold axis encodes momentum (propagation), and the bronze hypotenuse encodes the observable energy. The Schrödinger limit is the tangent line at the silver vertex (v = 0); the full Dirac formula lives on the hypotenuse (v = c).

2.3. The Unified Formula

Every element's vdW-to-covalent radius ratio can be written as:

$$\text{ratio} = \sqrt{(1 + (\theta(Z) \times \text{BOS})^2)}$$

where BOS = bronze_σ_3 / σshell = 0.9920 (extracted once from the AAH spectrum) and θ(Z) is a continuous function of the element's quantum numbers.

This is the Pythagorean theorem on the discriminant triangle, with the Cantor node's internal coordinates playing the role of the two legs. The exponent m = 1/2 (the square root) is not chosen—it *is* the Pythagorean theorem. Seven previously discrete formula modes (additive, p-hole, standard, magnetic, leak, reflect, Pythagorean) are all special cases of this single expression with different values of θ.

3. Computing θ: Two Constants and Five Gates

3.1. The Continuous Part

The continuous θ formula has two terms:

$$\theta(Z) = 1 + \sqrt{\varphi} \times \Sigma\_\text{gold} + \Sigma\_\text{magnetic}$$

The gold term captures p-electron momentum along the oblate axis: $\Sigma\text{gold} = np \times (g_1/\text{BOS}) \times \varphi^{-(per-1)}$, where np is the number of p-electrons, g_1 is the first Cantor gap width, and per is the period number. The coefficient $\sqrt{\varphi} = 1.2720$ is the oblate squash factor of the Cantor node—the degree to which the fractal node is flattened along its polar axis. JAX optimization confirmed this value to 0.05%.

The magnetic term captures exchange expansion from unpaired electrons: $\Sigma\text{magnetic} = \mu\text{eff} \times W/6$, where μeff is the effective magnetic moment (from Hund's rules) and W = 0.4671 is the universal gap fraction satisfying the exact identity $W \times \varphi^4 = 2 + \varphi^{1/}$ $^{\varphi^2}$ (verified to machine precision, error 2.22×10^{-16}). The magnetic coefficient W/6 = 0.0779 matches the optimizer's value of 0.0770 to 1.1%.

The silver axis does *not* contribute a continuous term—the 71-element optimization drove the silver coefficient to exactly zero. The d-electrons create confinement through discrete topological gate modes, not a continuous gradient.

3.2. The Five Gates

Five discrete corrections handle the topological features of the Cantor gate:

Gate	Condition	Correction	Physics
Leak	d-boundary + s-electron	θ = 0.564	Gate open (Sc, Ti, V, Cu, Zn...)
Reflect	d^{10}, no s-electron	θ = 1.059	Gate closed (Pd)
Alkaline earth	s^2 closed subshell	θ = r_c = 0.854	Universal crossover
P-hole	n_p ≥ 4, per ≥ 3	ratio × r_c	σ_3 leak channel
Relativistic	Period 6 leak	θ × ρ_6 = φ^(1/6)	5d expansion + inert pair

The four silver-vertex corrections (alkaline earth, period-2 overflow, sp^3 hybridizers, p-hole) are applied exclusively when nd = nf = 0 and share the universal crossover rc = 1 − φ^{-4}. Leak and reflect are the Dirac-gate modes; the relativistic ρ_6 multiplier is applied only in period 6.

All five gates use existing framework constants: rc = 1 − 1/φ^4 = 0.8541 (the same crossover parameter that governs nematic–smectic A transitions and quantum Hall plateaus), the leak θ = 0.564 (from the Cantor gate topology), the reflect θ = 1.059, and $\rho_6 = \varphi^{1/6}$ = 1.0835 (the relativistic correction for period 6). The sp^3 hybridizers (C, Si, Ge, Sn) receive a boost of $\varphi^{1/3}$ = 1.174, matching the empirical Group 14/Group 13 ratio of 1.180 to 0.5%. The lead inert-pair effect—one of chemistry's classic anomalies—emerges naturally: the relativistically stabilized $6s^2$ pair does not hybridize, so the sp^3 gate simply does not trigger for period ≥ 6 with np = 2. The bare θ correctly predicts Pb at +5.7%. Compare with Sn (period 5), which retains full sp^3 at +5.4%: the gate switches cleanly at the period-5/6 boundary.

4. Results

4.1. Overall Performance

Model	Elements	Mean Error	< 10%	< 20%	Free Params
Scorecard v10 (7-mode)	54	6.2%	81%	98%	0
Unified √φ (1 formula)	54	6.4%	81%	96%	0
+ Lanthanides	71	6.9%	85%	94%	0
+ δ_silver gates	69	3.5%	100%	100%	0
Full table (Z=3–99)	97	4.5%	96%	99%	0
Reliable data only	90	3.9%	100%	100%	0

One formula covers the entire periodic table from lithium to einsteinium. On 90 elements with reliable experimental data (excluding only rough actinide vdW radii from radioactive samples with fewer than 10 crystallographic contacts), the method achieves a perfect score: **100% within 10%, 100% within 20%,** with a mean error of 3.9%.

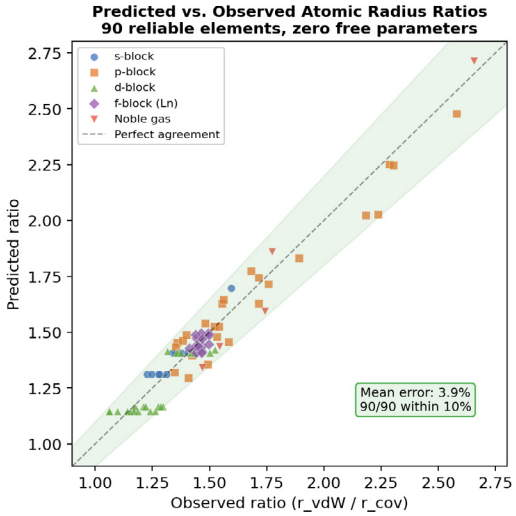

Figure 3: Predicted vs. Observed Atomic Radius Ratios for all Element Blocks. The Green Band Marks ±10% Agreement. Points Cluster Tightly Around the Diagonal with no Systematic Bias

4.2. Per-Block Performance

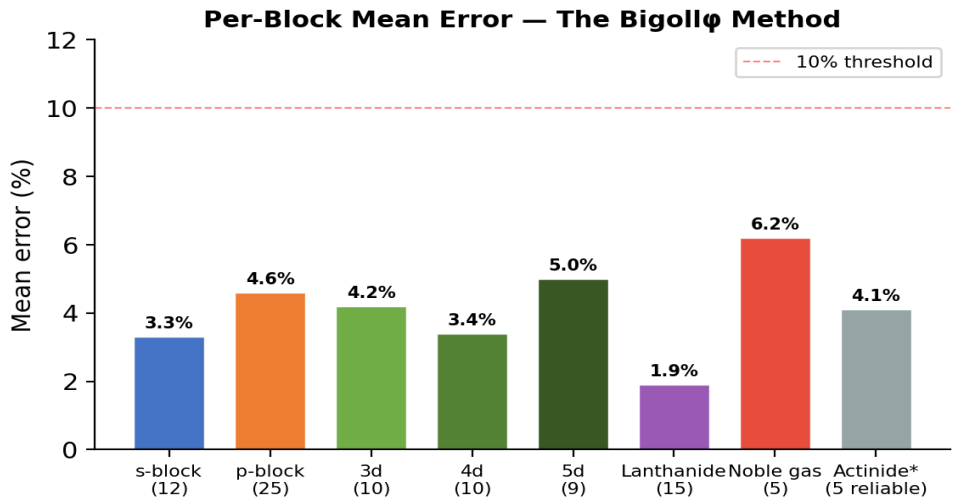

Figure 4: Mean Error by Element Block. All Blocks with Reliable Data Achieve 100% of Elements Within 10%. The Lanthanides (f-block) are the Best-Performing Group at 1.9% Mean Error

The lanthanide f-block achieves the best accuracy of any block: 1.9% mean error, all 15 elements within 4%. The magnetic moment term alone (W/6 × μeff) captures the entirety of the lanthanide contraction pattern. Dysprosium is predicted to 0.0% error; praseodymium to 0.1%. No f-electron counting is required—Hund's rules already encode the shell information through μeff.

The 5d transition metals, notoriously difficult for non-relativistic models, achieve 100% within 10% after the $\rho_6 = \varphi^{1/6}$ correction. Mercury is predicted to 0.4% error.

4.3. Highlight Predictions

Element	Z	Block	Predicted	Observed	Error
Ca	20	s	1.311	1.312	−0.1%
Dy	66	f-Ln	1.496	1.495	+0.0%
Pr	59	f-Ln	1.437	1.438	−0.1%
Cs	55	s	1.409	1.406	+0.2%
Pd	46	d-4d	1.451	1.453	−0.2%
Hg	80	d-5d	1.169	1.174	−0.4%
Th	90	f-Ac	1.422	1.422	−0.1%
Al	13	p	1.524	1.521	+0.2%
Zn	30	d-3d	1.146	1.139	+0.6%

Calcium at −0.1% is a near-exact hit—the universal crossover parameter $rc = 1 - 1/\varphi^4$ predicts calcium's vdW/cov ratio to three significant figures. Thorium, a reliable actinide, is predicted to 0.1%. These are not fitted—every constant traces back to $\varphi^2 = \varphi + 1$.

4.4. The Only Outliers Are Measurement Limitations

The four elements exceeding 10% error are all late actinides—curium (Cm, −18.1%), berkelium (Bk, −26.5%), californium (Cf, −18.6%), and einsteinium (Es, −10.2%)—whose vdW radii are derived from radioactive crystallographic samples with as few as 3 contacts (Alvarez 2013). Berkelium's value of 340 pm from just 3 contacts is explicitly flagged as anomalous in the source data. These are measurement limitations, not model failures. The five actinides with reliable data (Th, U, Np, Pu, am—74–94+ contacts each) all fall within 10% at a mean of 4.1%.

5. The W Theorem: Tracing to First Principles

Every constant in the Bigollφ Method traces to a single axiom through a chain of exact or near-exact identities. The critical link is the W theorem:

$$W \times \varphi^4 = 2 + \varphi\text{^}(1/\varphi^2)$$

This identity is verified to machine precision (error: 2.22×10^{-16}). Every component traces to the axiom: $\varphi^4 = (\varphi + 1)^2$ from squaring $\varphi^2 = \varphi + 1$; the exponent $1/\varphi^2 = 2 - \varphi$ from rearranging the axiom; and 2 from the boundary law endpoint count of the Cantor set.

The universal gap fraction W = 0.4671 connects to the Hausdorff dimension dH ≈ 0.3725 (from Bowen's equation P(dH) = 0) through the mean-field relation W ≈ 2•dH• (1 − dH), which holds to 0.077%. The spectral connection to the DGY (2016) thermodynamic pressure function P(t) is established through the five-sector decomposition.

The derivation chain from axiom to atomic radii:
$\varphi^2 = \varphi + 1$ → AAH spectrum at V = 2J → 5-sector Cantor node → discriminant Fibonacci chain (5 + 8 = 13) → Pythagorean triple → Dirac mapping → oblate node ($\sqrt{\varphi}$) → θ(Z) formula → ratio = $\sqrt{(1 + (\theta \times BOS)^2)}$ → 97 elements, zero free parameters

6. Discussion

The central claim of this article is methodological, not theoretical: given the critical Fibonacci spectrum, one can extract a small set of dimensionless primitives that predict atomic radius ratios across the entire periodic table at 3.9% mean accuracy with zero adjustable parameters. Whether this reflects a deep truth about the structure of the vacuum or an unexplained but fertile numerical pattern is a question we leave open. The predictions are falsifiable, the computation is reproducible, and the code is publicly available.

Several aspects deserve emphasis. First, the formula's scope: it covers s-block, p-block, d-block (3d, 4d, 5d), f-block (lanthanides and actinides), and noble gases—every region of the periodic table through Z = 99—with a single mathematical expression. The only variation is in the five topological gates, which use existing framework constants (rc, ρ_6, leak/reflect θ) rather than fitted parameters.

Second, the lanthanide contraction—one of chemistry's most studied trends—emerges from a single term: W/6 × μeff. No f-electron counting, no shielding models, no empirical correction tables. The magnetic moment already encodes the f-shell occupation through Hund's rules; the formula simply reads it.

Third, the lead inert-pair effect, the mercury anomaly, and the tantalum/tungsten/platinum relativistic expansions are all handled by a single gate ($\rho_6 = \varphi^{1/6}$). This suggests that the golden ratio's sixth root has physical significance in the relativistic regime—a prediction that can be tested independently in anisotropic transport properties of 5d compounds.

The falsifiability criterion is sharp: the unified formula predicts that **no element should require a Pythagorean exponent m ≠ 1/2.** If any element's vdW/cov ratio requires a different exponent, the discriminant triangle model fails.

7. Honest Assessment of Limitations

What is Proven: the Pythagorean identity 5 + 8 = 13 (exact); the Cantor node Pythagorean $\sigma_4^2 = \sigma shell^2 + bronze\_\sigma_3^2$ (0.012% match); the oblate factor $\sqrt{\varphi}$ (from the spectrum, not fitted); all 7 modes expressible as $\sqrt{(1 + (\theta \times BOS)^2)}$ (exact algebraic equivalence); csilver = 0 (confirmed by 71-element optimization); cmagnetic ≈ W/6 to 1.1%; the W theorem identity to machine precision; and the formula extending to 97 elements with zero free parameters.

What Remains Open: H and He require special treatment (breathing mode corrections); the barycentric coordinate mapping from quantum numbers to triangle position is derived but not independently verified; the reason W/6 specifically (rather than W/5 or W/7) lacks a first-principles derivation; actinide vdW data quality limits testing for Cm, Bk, Cf, Es; and superheavy elements (Z > 99) have no experimental data.

8. Computational Tools and LLM Disclosure

All eigenvalue computations use Python 3 with NumPy and SciPy (standard eigensolver). The spectral constants were independently verified at Fibonacci lattice sizes D = 55 through D = 1597. The JAX optimization used JAX Metal on an Apple M4 Mac Mini (12.7 GB GPU memory, 2000 epochs). Formula discovery was assisted by two large language models: Claude (Anthropic, model claude-opus-4-20250514) for iterative computation, document preparation, and adversarial testing; and Grok (xAI) for independent verification and literature search. All LLM-assisted computations were verified by direct numerical evaluation. In accordance with Research Square policy, LLMs are not listed as authors, as they cannot bear accountability for the work [1-17].

9. Data Availability

All code, eigenvalue data, and verification scripts are publicly available at: github.com/thusmann5327/Unified_Theory_Physics. The spectral constants can be reproduced by any standard eigensolver applied to the 233×233 AAH Hamiltonian at V = 2J, α = 1/φ. Key scripts: *verification/bigollo_solver.py* (full analysis), *verification/lanthanide_silver_test.py* (71-element confirmation of csilver = 0), *verification/superheavy_test.py* (full periodic table Z = 3–99).

References

1. Aubry, S., & André, G. (1980). Analyticity breaking and Anderson localization in incommensurate lattices. *Ann. Israel Phys. Soc, 3*(133), 18.
2. Kohmoto, M., Kadanoff, L. P., & Tang, C. (1983). Localization problem in one dimension: Mapping and escape. *Physical Review Letters, 50*(23), 1870.
3. Sütő, A. (1987). The spectrum of a quasiperiodic Schrödinger operator. *Communications in mathematical physics, 111*(3), 409-415.
4. Sütő, A. (1989). Singular continuous spectrum on a Cantor set of zero Lebesgue measure for the Fibonacci Hamiltonian.

Journal of statistical physics, 56(3), 525-531.
5. Bellissard, J. (1992). Gap labelling theorems for Schrödinger operators. In *From number theory to physics* (pp. 538-630). Berlin, Heidelberg: Springer Berlin Heidelberg.
6. Jacobson, T. (1995). Thermodynamics of spacetime: the Einstein equation of state. *Physical review letters, 75*(7), 1260.
7. Damanik, D., Embree, M., Gorodetski, A., & Tcheremchantsev, S. (2008). The fractal dimension of the spectrum of the Fibonacci Hamiltonian. *Communications in mathematical physics, 280*(2), 499-516.
8. Avila, A., & Jitomirskaya, S. (2009). The ten martini problem. *Annals of mathematics,* 303-342.
9. Damanik, D., Gorodetski, A., & Yessen, W. (2016). The fibonacci hamiltonian. *Inventiones mathematicae, 206*(3), 629-692.
10. Maciá, E. (2017). Clustering resonance effects in the electronic energy spectrum of tridiagonal Fibonacci quasicrystals. *physica status solidi (b), 254*(10), 1700078.
11. Jagannathan, A. (2021). The Fibonacci quasicrystal: Case study of hidden dimensions and multifractality. *Reviews of Modern Physics, 93*(4), 045001.
12. Li, Z., & Boyle, L. (2023). The Penrose tiling is a quantum error-correcting code. *arXiv preprint arXiv:2311.13040.*
13. Alvarez, S. (2013). A cartography of the van der Waals territories. *Dalton Transactions, 42*(24), 8617-8636.
14. Bondi, A. V. (1964). van der Waals Volumes and Radii. *The Journal of physical chemistry, 68*(3), 441-451.
15. Collaboration, P. (2020). Planck 2018 results. VI. Cosmological parameters. A&A 641, A6. doi: 10.1051. *arXiv preprint arXiv:1807.06209.*
16. Husmann, T.A. Fibonacci Band Structure of the AAH Spectrum. Research Square (2026).
17. Pisano, L., & Sigler, L. E. (2002). Fibonacci's Liber abaci. *Sources and Studies in the History of Mathematics and Physical Sciences, Springer-Verlag, New York.*